Inorganic Chemistry

Award Paper

pubs.acs.org/IC

Inorganic Electron Transfer: Sharpening a Fuzzy Border in Mixed Valency and Extending Mixed Valency across Supramolecular Systems

Clifford P. Kubiak*

Department of Chemistry and Biochemistry, University of California, San Diego (UCSD), 9500 Gilman Drive, MC 0358, La Jolla, California 92093, United States

ABSTRACT: This article describes research from our laboratory on the chemistry and spectroscopic properties of inorganic mixed-valence complexes. After a brief review of the seminal work of Taube, Creutz, Day, Robin, Hush, and others in the 1960s and the confounding efforts to identify the borderline between class II and III mixed-valence systems in the 1990s and early 2000s, we describe our first experiments to observe and analyze the coalescence of ν(CO) band shapes in the 1D IR spectra of mixed-valence complexes of the type $\{[Ru_3O(OAc)_6(CO)(L)]_2\text{-BL}\}^-$, where L = a pyridyl ligand and BL = pyrazine or 4,4′-bipyridine, to estimate rate constants of intramolecular electron transfer (ET). The strong involvement of the bridging ligands in mixed-valence complexes of this type was first identified in the appearance of totally symmetric vibrational modes of pyrazine bridging ligands in the IR because of strong vibronic coupling within a three-state metal cluster−bridge−metal cluster model. Application of the Brunschwig−Creutz−Sutin semiclassical three-state model of mixed valency accounts well for the appearance of two intervalence charge-transfer bands that are observed in the near-IR region of the electronic absorption spectra of these mixed-valence ions. The direct spectroscopic observation of "mixed-valence isomers", the two alternate charge distributions of a mixed-valence ion, are described. The equilibrium constants of mixed-valence isomers provide quantitative thermodynamic estimates of the electronic coupling, H_{ab}. The extent of delocalization in many of the mixed-valent bridged dimers of triruthenium clusters produces unusual behavior, especially rate constants for ET that are independent of normal solvent reorganization energies but do depend on solvent dynamical dipolar reorientation times. The strong dependence of rates on solvent dynamics is also found to produce a non-Arrhenius dependence of ET rate constants on temperature, faster rates in frozen solutions compared to fluid solutions. The studies of these mixed-valence systems have provided generalized guidelines for establishing where a particular mixed-valence system lies along the class II/III delocalization transition, and they have increased our understanding of the ET dynamics at the delocalization threshold.

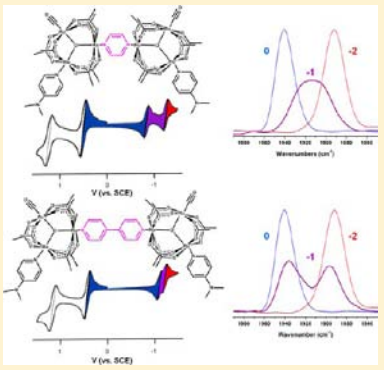

INTRODUCTION

Mixed valency has been a core problem in inorganic chemistry for over 40 years. The Creutz−Taube ion is the first example of the deliberate synthesis of an inorganic mixed-valence system.[1] It is interesting to look back at the title of the original communication from Creutz and Taube: "A Direct Approach to Measuring the Franck−Condon Barrier to Electron Transfer between Metal Ions". Today, the Creutz−Taube ion is considered to be one of the most important and iconic examples of inorganic synthesis, but in 1969, its significance was seen by the authors to be the observation in the near-IR of what we now call the intervalence charge-transfer (IVCT) electronic transition. In subsequent years, Hush[2] and Sutin[3,4] would add much to the Marcus theoretical framework for electron transfer (ET) to give the now familiar two-state model of mixed valency, parametrized in terms of the reorganization energy, λ, the electronic coupling, H_{ab}, and the thermal barrier to ET, E_{th}, for a reaction with no driving force (Figure 1). Hush, in particular, described how the extent of donor−acceptor electronic coupling, H_{ab}, could be determined from the energy and shape of the IVCT band.[2] Since the beginning, one of the most elementary questions about mixed valency has also been one of the most difficult to answer, and that is the question of the precise extent of delocalization. The most widely accepted and applied method is the Robin−Day mixed-valence classification.[5] This method classifies mixed-valence complexes in three classes based on the extent of electronic coupling: class I (uncoupled, $H_{ab} = 0$), class II (moderately coupled, $0 < H_{ab} < \lambda/2$), and class III (delocalzed, $H_{ab} \geq \lambda/2$). The strong integration of synthesis, spectroscopy, and theory was evident at the very beginning of the field of inorganic mixed valency, and this has kept it strong and broadly scientifically relevant ever since. However, although the Robin−Day classifications have been applied to many systems and verified by various experimental methods,[6−12] describing the precise character of mixed-valence complexes that lie on the class II/III borderline has been a particularly challenging problem over the past decade.[8,9,13−20]

Received: October 24, 2012
Published: January 15, 2013

   dx.doi.org/10.1021/ic302331s | *Inorg. Chem.* 2013, 52, 5663−5676

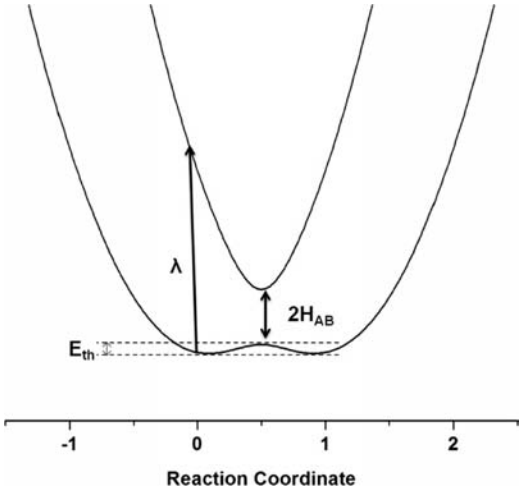

Figure 1. Marcus–Hush two-state potential energy surface for ET with no driving force as in a symmetric mixed-valence complex, parametrized in terms of the reorganization energy, λ, the electronic coupling, H_{ab}, and the thermal barrier to ET, E_{th}.

The difficulty of distinguishing between various shades of delocalization along the class II/III spectrum of possibilities may seem perplexing, even when considered in the simplest terms. At that level, the relevant questions are as follows: (1) Is the potential energy surface characterized by a single minimum (delocalized) or two (localized) minima? (2) If there is a double minimum, what is the barrier to ET? In the case of a double minimum, the barrier would be reflected in the rate. So, by determining the rates of ET, one would be able to describe some important details of the ground-state potential energy surfaces. It is very interesting and significant that the rate of ET in the Creutz–Taube ion has never been measured. Of course, it is not an easy experiment to do. ET in a symmetric mixed-valence complex is a degenerate exchange reaction, so there is no net chemical change. You end up with exactly what you started with, and so unraveling or probing the dynamics of such a reaction can be very difficult, indeed. One of our first contributions to this field was the introduction of a spectroscopic method for estimating the rates of ET in mixed-valence complexes, when the rates are very fast.[21,22]

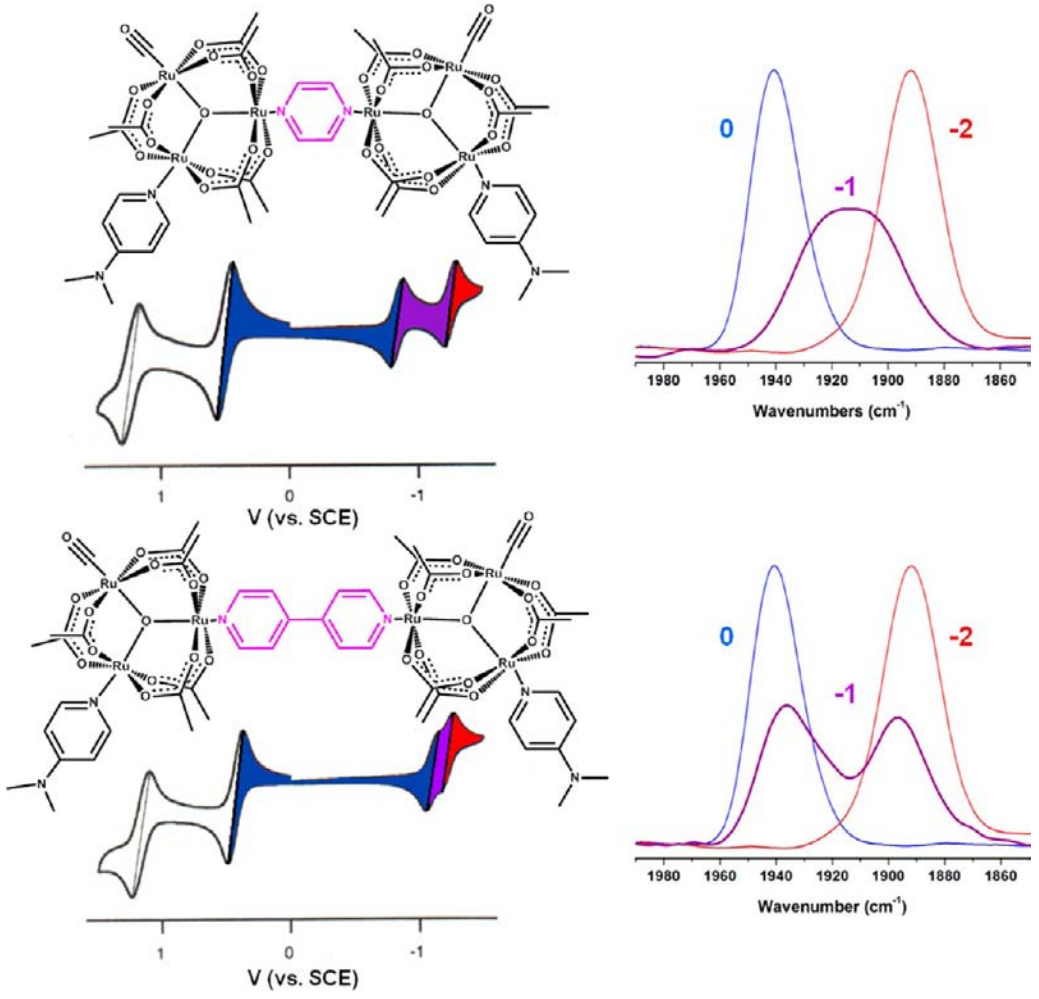

Figure 2. Structure, electrochemistry, and IRSEC responses for mixed-valence systems consisting of dimers of the Ru_3 clusters described. Highlighted are the varying bridging ligand, either pz or bipy, and their effects on electrochemical splitting on the reduction side of the CV, as well as on the coalescence of ν(CO) in the IR for the mixed-valence state. The colors of the ν(CO) spectra correspond to the redox states 0 (blue), 1– (purple), and 2– (red) and to the potential regions shaded in the CV (left) at which the spectra were collected.

dx.doi.org/10.1021/ic302331s | Inorg. Chem. 2013, 52, 5663–5676

IR SPECTROELECTROCHEMISTRY (IRSEC) AND COALESCENCE OF SPECTRAL LINE SHAPES

The application of IRSEC to study intramolecular ET in inorganic mixed-valence complexes came about from a chance meeting between the author and Prof. Tasuku Ito of Tohoku University at a conference in Taipei in 1995. Our laboratory had developed an IRSEC cell for measuring IR spectra through a thin-layer solution sample in reflectance mode, where the reflector is a polished platinum working electrode disk. We were using the IRSEC cell to study carbon dioxide reduction catalysts.[23−26] Ito's laboratory was studying the redox chemistry of basic ruthenium acetate oligomers, some of which had 11 reversible processes evident in their cyclic voltammograms (CVs).[27,28] We began our collaboration with IRSEC studies of mixed-valence complexes of the type $[Ru_3(\mu_3\text{-}O)(OAc)_6(CO)(L)(\mu_2\text{-}BL)Ru_3(\mu_3\text{-}O)(OAc)_6(CO)(L)]^-$, where L = a pyridyl ligand and BL = pyrazine (pz) or 4,4′-bipyridine (bipy), and published our first paper together in 1997.[21] It was because these clusters had carbon monoxide ligands in them that we were able to employ the coalescence of ν(CO) bands to estimate the dynamics of ET. The method is analogous to the use of dynamic NMR to study fluxional processes.[29] The frequency between two chemical shifts can be used to determine the dynamics of a chemical exchange process that causes spectral coalescence. In general, spectral line-shape coalescence requires that the rate of the dynamic process that causes exchange occurs at approximately the *difference* in frequency between the two spectral bands of interest in the absence of exchange.

The use of coalescence of IR spectra had been employed to study the dynamics of several different types of exchange processes, prior to our work. One of the often-discussed shortcomings of the method is the fact that there are many contributions to IR line shapes and whether it is possible to extract the dynamics of chemical exchange from the other operative line-broadening processes. Strauss has argued that "pseudocollapse", the progressive broadening of bands arising from an anharmonic potential, causes shifts and broadening of bands in the vibrational spectra that are not due to a chemical exchange reaction.[30] Certainly, the most important and well-known examples of "dynamic IR" are the studies of (η^4-diene)$Fe(CO)_3$ systems that were reported to undergo turnstile-like pseudorotation on the picosecond time scale by Grevels and Turner.[31−34] The work of Cannon on triiron acetate clusters is also particularly relevant.[35−37] Dynamic 1D IR band-shape coalescense has also been reported in the delocalized states of poly(aniline) and poly(2-phenoxy-*p*-phenylenevinylene) conducting polymers.[38]

Time-resolved 2D IR spectroscopy is a very promising method to study very fast dynamical processes, such as those of interest in our work. There are two widely employed techniques in the 2D IR community: vibrational-echo 2D IR[39,40] and dynamic hole burning, or double-resonance 2D IR.[41,42] Although much progress has been made in the implementation and studies of systems of 2D IR, there have only been a few examples of the direct study of ET by 2D IR.[43−47] While there are clear risks of using Bloch line-shape analysis from NMR spectroscopy for extracting ET rates from the dynamic coalescence of vibrational bands in IR spectra, there are also some advantages. The method can, in the limit of a few competing line-broadening processes, provide a self-consistent approximation of ET rates. These approximate rates do agree with the time scales of the dynamics that influence them, such as solvent relaxation (vide infra), and the technique is fast and does not require expensive or highly specialized instrumentation.

The IRSEC experiment, as applied to $\{[Ru_3O(OAc)_6(CO)(L)]_2\text{-}BL\}^-$, where L = a pyridyl ligand and BL = pz or bipy mixed-valence systems, proceeds as follows (Figure 2). We consider the CVs first. In the neutral resting states, each ruthenium cluster is in the $Ru_3^{III,III,II}$ redox state, with the carbon monoxide ligand on the formally d^6 ruthenium(II) center. On the oxidative side of the electrochemistry, the first process observed is the two-electron (double-current) oxidation of both $Ru_3^{III,III,II}$ clusters to their $Ru_3^{III,III,III}$ states. At more positive potentials, a second two-electron process is observed that converts $Ru_3^{III,III,III}$-BL-$Ru_3^{III,III,III}$ to $Ru_3^{III,III,IV}$-BL-$Ru_3^{III,III,IV}$. The μ-oxo center stabilizes the formally ruthenium(IV) states. The reductive side of the electrochemistry is very informative of the intercluster mixed-valence interactions between the two Ru_3 clusters and has allowed us to better understand the thermodynamics of these systems. The reductions occur as sequential one-electron processes that correspond formally to $Ru_3^{III,III,II}$-BL-$Ru_3^{III,III,II}$/$Ru_3^{III,III,II}$-BL-$Ru_3^{III,II,II}$ (0/1− overall charge) and then $Ru_3^{III,III,II}$-BL-$Ru_3^{III,II,II}$/$Ru_3^{III,II,II}$-BL-$Ru_3^{III,II,II}$ (1−/2− overall charge). The magnitude of the splitting between the 0/1− and 1−/2− reduction waves (ΔE = 435 mV) in the L = 4-(dimethylamino)pyridine (dmap) and BL = pz case corresponds to the comproportionation constant, $K_c = 2.3 \times 10^7$, which is a direct measure of the relative thermodynamic stability of the mixed-valence (1−) state compared to the two isovalent (0 and 2−) states. The lower half of Figure 2 shows the CV of the BL = bipy system. The ΔE value between the first and second reduction waves is only about 120 mV, corresponding to $K_c = 1.1 \times 10^2$. The comparison of the K_c values is experimental evidence that the mixed-valence ion with BL = bipy is much less stable compared to the BL = pz case. The electrochemical value of ΔE is also related to the electronic coupling H_{ab} but only reliably when the effects of exchange outweigh the electrostatic effects in the charged ions.[48−51]

Additional spectroscopic information is provided by the IRSEC method. We continue with the comparison between the IRSEC responses of the complexes with BL = pz versus bipy, with L = dmap in both cases (Figure 2). IRSEC provides a method to quickly obtain the IR spectrum of each of the three relevant redox states: 0/1−/2−. At potentials corresponding to the neutral state, a single ν(CO) band at ca. 1940 cm^{-1} is observed, reflecting the fact that both of the carbon monoxide ligands reside in identical ($Ru_3^{III,III,II}$) redox environments. When both the first and second reduction waves are traversed, both clusters are reduced, and again a single ν(CO) band is observed, but at lower frequency, ca. 1890 cm^{-1}. This reflects the fact that both Ru_3 clusters are in identical ($Ru_3^{III,II,II}$) redox environments. For the BL = bipy case, it is possible to observe the 1− mixed-valence state when the potential of the IRSEC cell is poised between the first and second reduction waves. The bipy-bridged mixed-valence ion exhibits two ν(CO) bands, and they appear very much like a composite of the bands observed in the isovalent states. This is evidence that this particular mixed-valence ion is localized on the IR spectroscopy time scale. The pz-bridged mixed-valence system shows very different behavior. Besides the larger splitting ΔE between the two reduction waves in the CV, which indicates a much more stable mixed-valence ion, the ν(CO) band in the 1− mixed

dx.doi.org/10.1021/ic302331s | *Inorg. Chem.* 2013, 52, 5663−5676

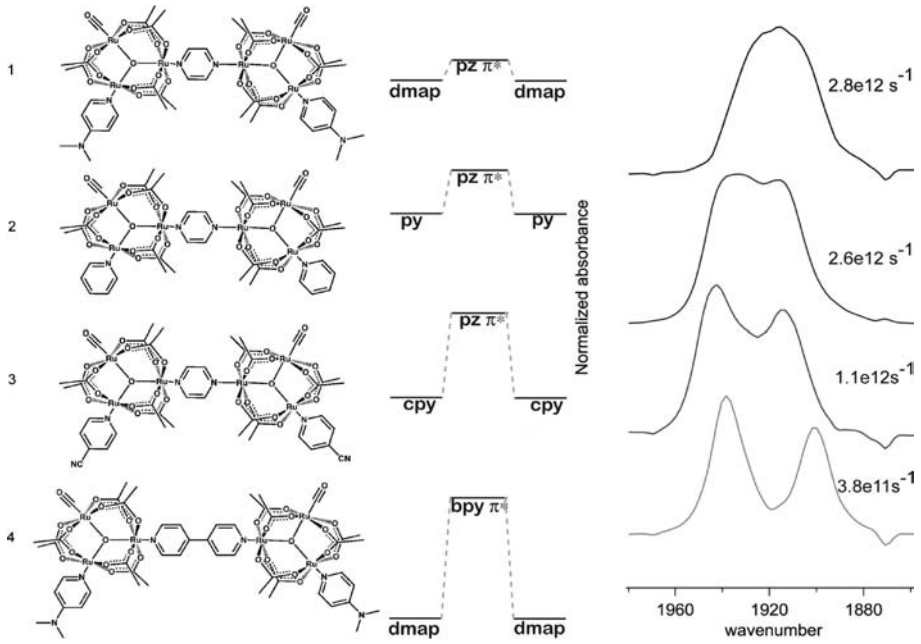

Figure 3. Summary of the structures, simplified electronic structures, and IR spectra in the ν(CO) region for four complexes: (left) Structural drawings of the systems studied, $[Ru_3(\mu_3\text{-}O)(OAc)_6(CO)(py)(\mu_2\text{-}BL)Ru_3(\mu_3\text{-}O)(OAc)_6(CO)(py)]^-$, where BL = pz and py = dmap (**1**), py (**2**), or cpy (**3**) and BL = bipy and py = dmap (**4**). (middle) Qualitative molecular orbital representations of the relative energies of Ru_3 d orbitals (LUMO for neutral species) and bridging ligand π^* orbitals. (right) ν(CO) region of the IR spectra of the mixed-valence ions $\mathbf{1}^-$–$\mathbf{4}^-$ in acetonitrile at 298 K, and rate constants, k_{ET}, estimated by simulation of the IR line shape.

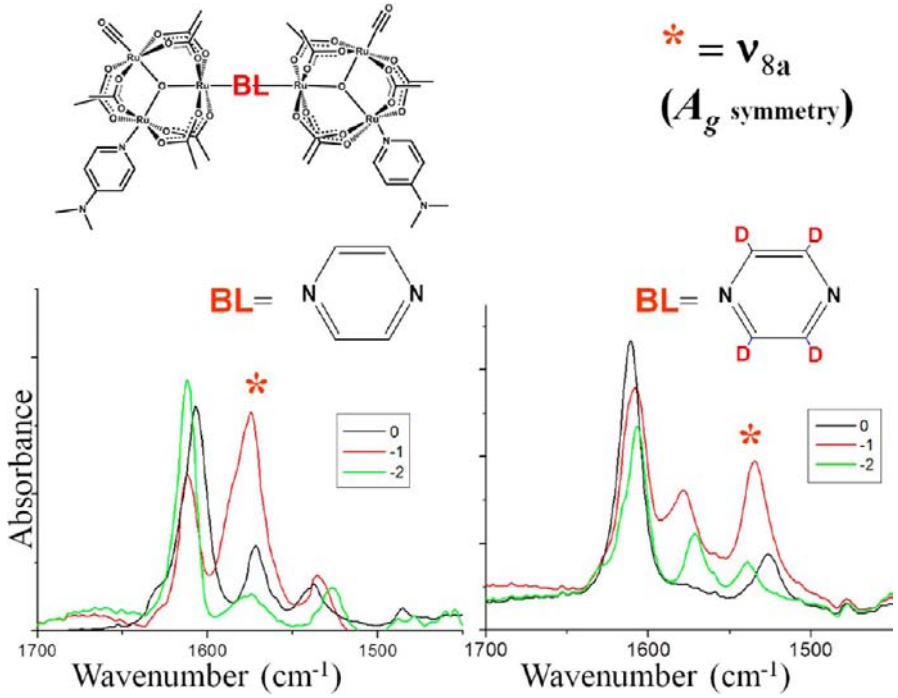

Figure 4. IR spectra of the complex $[Ru_3(\mu_3\text{-}O)(OAc)_6(CO)(dmap)(\mu_2\text{-}BL)Ru_3(\mu_3\text{-}O)(OAc)_6(CO)(dmap)]$ in the neutral (0; black), mixed-valence (1−; red), and fully reduced (2−; green) states for BL = pz (left) and pz-d_4 (right).

valence state is nearly a single Gaussian IR band. The coalesced IR line shape indicates that this mixed-valence ion is effectively delocalized on the IR time scale. Exchange on the IR time scale implies that when two bands are separated by 50 cm^{-1}, they are separated by 1.5×10^{12} s^{-1} in frequency, and this must then be the approximate time scale of the exchange process that causes coalescence. This is an indication that ET is occurring on the picosecond time scale.

The rates of intramolecular ET estimated by the IRSEC method are found to be influenced by a variety of factors including the electronic structure,[21,22,52] solvent,[17−19,53] and temperature.[17] Electronic structural effects are evident in the results of simple substitution of the ancillary ligands. When the ancillary ligands are changed from dmap to pyridine (py) to 4-cyanopyridine (cpy), the stronger donors give more coalesced ν(CO) spectra in the 1− states, indicating more delocalized

dx.doi.org/10.1021/ic302331s | Inorg. Chem. 2013, 52, 5663−5676

mixed-valence states. This is explained by an electronic structural model that places the Ru dπ levels of the mixed-valence ions just below the π^* levels of the pz bridging ligand.[52] Thus, in the language of ligand-field theory, as you place stronger donor ligands on the Ru_3 clusters, the d manifold rises in energy and into closer energetic alignment with the BL π^* levels, leading to more resonant delocalization across the mixed-valence ion. Figure 3 presents the structures of four mixed-valence ions, BL = pz and L = dmap (**1**), py (**2**), and cpy (**3**) and BL = bipy and L = dmap (**4**) (left), the presumed relative placement of Ru d and BL π^* levels (center), and the ν(CO) spectra recorded by IRSEC in the mixed-valence (1−) states (right). Rate constants are estimated from the measured line shape of the ν(CO) spectrum by spectral simulation. McClung's VIBEXGL follows the Bloch equation treatment of dynamic line-shape simulation normally used in NMR but with Gaussian, rather than Lorentzian, line shapes.[54] The routine involves computing line shapes for several assumed (ET) rate constants and selecting the simulated spectrum that agrees best with the experimental spectrum. The rate constants obtained by such simulations for the four mixed-valence systems depicted in Figure 3 are given on the right side of the experimental spectra in the figure. A key point is that the dynamic IR method is best suited for the study of extremely fast processes, those that occur on the picosecond time scale. This time scale is usually referred to as "ultrafast" in the physical chemistry community. The BL = bipy complex (**4**) in Figure 3 has two well-resolved bands in the IR spectrum, and this corresponds to a rate constant of about 4×10^{11} s^{-1}. By tuning the donor properties of the ancillary pyridine ligands and bringing the Ru d and BL π^* levels into closer energetic coincidence, the ν(CO) spectra become more coalesced, corresponding to faster ET rate constants in **1**−**3**. One can easily extrapolate this trend in behavior to conclude that complete coalescence, approaching what we call the fast-exchange limit in NMR, would require rate constants that are faster than 10^{12} s^{-1}.

IMPORTANCE OF THE BRIDGING LIGAND AND APPLICATION OF THE THREE-STATE MODEL OF MIXED VALENCY

Early in our studies of mixed valency in the Ru_3-BL-Ru_3 systems, some of the limitations of the two-state model for mixed valency (Figure 1) became evident. We were forced to consider more detailed models of the electronic structure that explicitly included the bridging ligands. For example, one puzzling feature of the IR spectra of these systems was that the totally symmetric stretch of pz (ν_{8a}) was clearly evident in the IR spectrum.[55] Interestingly, the ν_{8a} mode only showed significant intensity in the mixed-valence states. Figure 4 compares the IR spectra of the complex $\{[Ru_3O(OAc)_6(CO)(py)]_2\text{-BL}\}^-$ in the neutral (0), mixed-valence (1−), and fully reduced (2−) states for BL = pz (**2**) (left) and pz-d_4 (right). The pz ν_{8a} mode is found to be significantly overlapped with other bands in the IR spectrum for the naturally isotopically substituted ligand. However, when the deuterated ligand pz-d_4 is used, the ν_{8a} mode becomes well-separated from the other bands and is clearly observable. It is then evident that only in the mixed-valence state does the ν_{8a} mode show a significant increase in intensity compared to the bands in the same region of the isovalent states. Meyer et al. have discussed this as an example of symmetry breaking that is taken as evidence for localization; i.e., if the electron is localized in the mixed-valence ion, then the pz bridging ligand would be placed in an asymmetric environment.[9] This could give oscillator strength to a normally forbidden totally symmetric IR mode. We, and others, have investigated this possibility through combined synthetic and resonance Raman spectroscopic studies.[56−58] One important observation involved the η^1-pyrazine complex, $Ru_3(\mu_3\text{-O})(OAc)_6(CO)(dmap)(\eta^1\text{-pz})$, where only one end of the pz ligand is coordinated to a Ru_3 complex. This complex clearly contains a pz ligand in an asymmetric environment, but it shows negligibly small intensities in the vicinity of the ν_{8a} mode in all three of its redox states (1+/0/1−).[55] There now seems to be agreement that the intensification of the ν_{8a} mode in the mixed-valence states of the $[Ru_3(\mu_3\text{-O})(OAc)_6(CO)(L)\text{-(pz)-}Ru_3(\mu_3\text{-O})(OAc)_6(CO)(L)]$ complexes results from strong vibronic coupling between the pz bridging ligand and the Ru_3-based electronic states.[58] The intensity enhancement of the normally IR-forbidden ν_{8a} mode of the pz bridging ligands is a consequence of mixing of vibrational and electronic transitions through vibronic coupling in a three-state (Ru_3-BL-Ru_3) model. The result of this mixing is that the pure $|0\rangle \rightarrow |1\rangle$ transition of the symmetric bridging ligand vibration can acquire dipole activity from the electronic transition to which it is coupled. This implies that the observation of formally forbidden bridging ligand modes in IR spectra is a marker of vibronic coupling and a strong interaction of the metal centers with the bridging ligand in mixed-valence complexes including the Creutz−Taube ion and those discussed here. Clearly, this is a completely different physical model for the appearance of symmetric modes of vibration in the IR than the symmetry breaking localization versus delocalization at the class II/III borderline. Resonance Raman experiments conducted on the mixed-valent dimers of Ru_3 clusters show strong enhancement of the totally symmetric modes of vibration of the pz bridging ligand, which is consistent with the vibronic coupling three-state description of these systems.[56,57]

Understanding the importance of the bridging ligands also is required in the assignment of the IVCT electronic transitions in the near-IR region. The assignment of the IVCT bands has been revised several times since they were first observed and described.[22] Initially, only the lowest-energy band at ca. 7000−8000 cm^{-1} (Figure 5) was assigned as the unique two-state IVCT band of the series of mixed-valence ions (**1**−**4**) shown. As we studied these systems further, it soon became clear that there were really *two* IVCT bands: the low-energy bands at ca. 7000−8000 cm^{-1} and higher-energy bands at 9525−11110 cm^{-1} (Figure 5).[52] As the need for a three-state model became apparent from the vibronic enhancement of symmetric modes of vibration in the IR spectra of mixed-valence states, we adopted the three-state vibronic coupling model of Ondrechen et al.[11] The three-state vibronic model predicted the enhancement of symmetric modes of vibration of bridging ligands in the mixed-valence states and also the appearance of two IVCT bands.[59] The model did not, however, provide a qualitative means of describing how increasing degrees of electronic communication (H_{ab}) affected the energies of the two IVCT bands. The semiclassical three-state model of mixed valency described by Brunschwig et al.[13] provided a better description of the observed IVCT bands of these systems. The Brunschwig−Creutz−Sutin ("BCS") semiclassical three-state model predicts the appearance of two IVCT bands, one metal-to-metal (MMCT) and the other metal-to-bridge (MBCT) charge transfer in character. The basic principles of the BCS semiclassical model are summarized in Figure 6. Three potential energy surfaces arise from the interaction of two

dx.doi.org/10.1021/ic302331s | Inorg. Chem. 2013, 52, 5663−5676

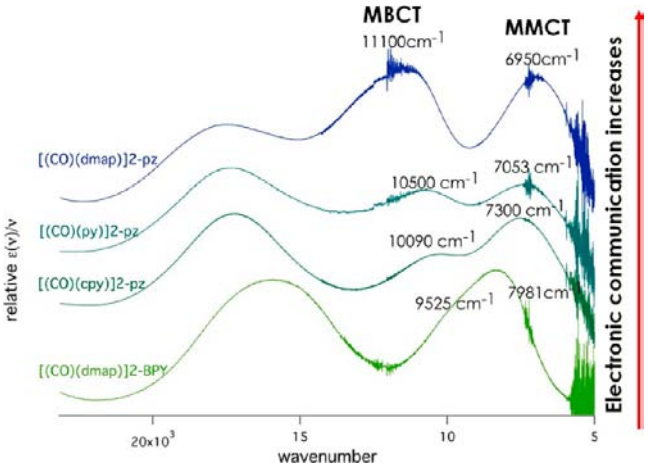

Figure 5. Near-IR spectra of mixed-valence complexes $\{[Ru_3O(OAc)_6(CO)(L)]_2\text{-BL}\}^-$, where BL = pz and L = dmap (**1**), py (**2**), and cpy (**3**) and BL = bipy and L = dmap (**4**) in acetonitrile at 298 K. Band energies are given, showing the trends observed with increasing electronic communication based on ancillary ligand substitution. Spectra are offset for clarity.

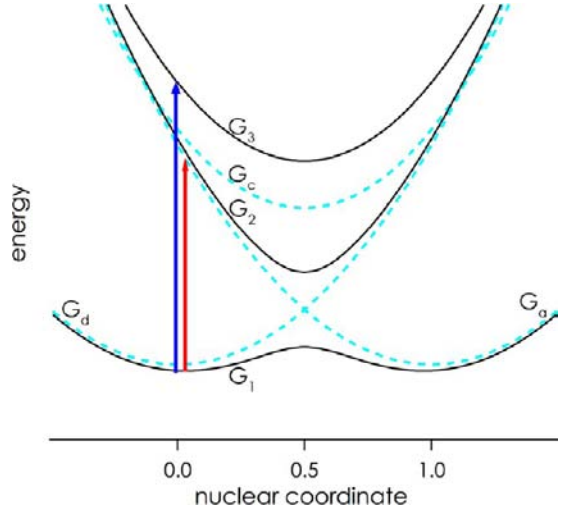

Figure 6. Three-state semiclassical potential energy surfaces following BCS that arises from the interaction of two metal-based diabatic surfaces for the donor (G_d) and acceptor (G_a) and a third diabatic surface for the bridging ligand, G_c. Three adiabatic states result: the ground state, G_1, from the symmetric combination of metal-based states, an excited state G_2 from the antisymmetric combination of metal-based states, and a second excited state, G_3, derived mostly from the bridging ligand. When the bridging ligand states are known to lie above the metal-based states in energy, two electronic transitions are predicted: MMCT shown in red at lower energy and MBCT shown in blue at higher energy.

metal-based diabatic surfaces for the donor (G_d) and acceptor (G_a) and a third diabatic surface for the bridging ligand, G_c. Three adiabatic states result: the ground state, G_1, from the symmetric combination of metal-based states, an excited state, G_2, from the antisymmetric combination of metal-based states, and a second excited state, G_3, derived mostly from the bridging ligand. When the bridging ligand states are known to lie above the metal-based states in energy, as they are from the ancillary ligand substitution effects on the rates of ET (Figure 3), two electronic transitions are predicted: MMCT, shown in red at lower energy, and MBCT, shown in blue at higher energy in Figure 6. The three-state model requires two electronic couplings: metal donor−acceptor (H_{ad}, using the labels in Figure 6) and metal donor−bridge (H_{ac}). Figure 7 shows the average effects of increasing the metal donor−acceptor and metal−bridge couplings. It can be seen that, as the overall electronic communication increases (increase in both H_{ad} and H_{ac}) and the potential energy surfaces move toward delocalization (single minimum), two things happen: the energy of the MMCT transition moves to lower energy and the MBCT transition moves to higher energy.

We now consider how the BCS three-state model applies to the IVCT spectra of the mixed-valence ions of the form $\{[Ru_3O(OAc)_6(CO)(L)]_2\text{-BL}\}^-$. Figure 5 shows visible and near-IR spectra of mixed-valence complexes $\mathbf{1}^-$−$\mathbf{4}^-$. The high-energy bands (ca. 18000 cm^{-1}) correspond to intracluster MLCT bands and are not pertinent to this discussion. Following the preceding discussion, the lowest-energy IVCT bands of $\mathbf{1}^-$−$\mathbf{4}^-$, observed at ca. 7000−8000 cm^{-1}, are assigned as MMCT in origin and the higher energy bands at 9525−11100 cm^{-1} are assigned as MBCT. The three-state model predicts that these bands will display the following characteristic behaviors as the electronic communication increases: diverging energies between MMCT (down) and MBCT (up) bands, intensification of the MMCT band, and spectral cutoff on the low-energy side of the MMCT band.[13] This behavior is precisely what is observed for the MMCT and MBCT spectra for $\mathbf{1}^-$−$\mathbf{4}^-$ (Figure 5). Importantly, the divergence in energy of the MMCT and MBCT bands and intensification of the MMCT band are clear indications of increased delocalization. This can be seen in the progression of the most to the least delocalized mixed-valence ions in the order $\mathbf{1}^- > \mathbf{2}^- > \mathbf{3}^- \gg \mathbf{4}^-$. The response of the MMCT and MBCT bands to temperature and solvent can provide even more significant information about where a particular mixed-valence ion lies on the transition from localization to delocalization at the class II/III borderline.

"MIXED-VALENCE ISOMERS" AND OBSERVATION OF THE TWO DISCRETE CHARGE DISTRIBUTIONS IN A MIXED-VALENCE ION

The extent of delocalization of a mixed-valence ion can be seen in the profile of the ground-state potential energy surface. We have endeavored to experimentally determine the energy differences between the most prominent features of the ground-state potential energy surfaces of mixed-valence complexes. By the synthetic introduction of small asymmetries into the structures of mixed-valence ions, it is possible to introduce small energy differences between the two sides of the Marcus−Hush (or BCS) potential energy surfaces. In some cases, these energy differences can be so small that both mixed-valence isomers exist in equilibrium.[60,61] This was achieved in two different ways. The first method employs an asymmetric bridging ligand, BL = 2-methylpyrazine (2-mpz), and mixed-valence isomers are observed in the IR by selective isotopic substitution of the carbonyl ligands.[61] This required the regioselective substitution of $^{13}C^{18}O$ onto one side of the dimer of trimers, either syn or anti to the mpz group. The synthesis involves the metal complex in a ligand synthetic approach (Figure 8). The monoancillary-substituted solvento species, $Ru_3(\mu_3\text{-O})(OAc)_6(CO)(py)(solvent)$, is reacted with the 2-mpz ligand.[62] This reaction proceeds under kinetic control with the less substituted side of the 2-mpz group binding to ruthenium. The resulting complex, $Ru_3(\mu_3\text{-O})$-

dx.doi.org/10.1021/ic302331s | Inorg. Chem. 2013, 52, 5663−5676

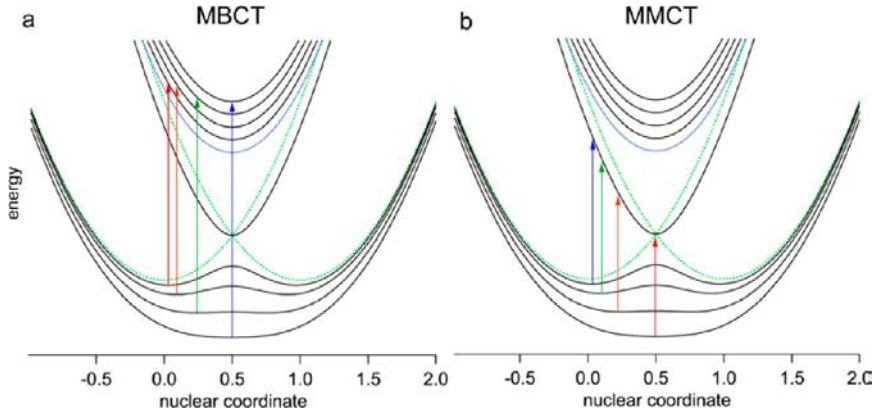

Figure 7. Potential energy surfaces showing the effect of increased coupling on the MBCT energy of adiabatic ground and bridge states (a) and the effect of increased coupling on the MMCT energy of adiabatic ground and excited metal states (b). Increased coupling leads to more energetic MBCT bands and less energetic MMCT bands.

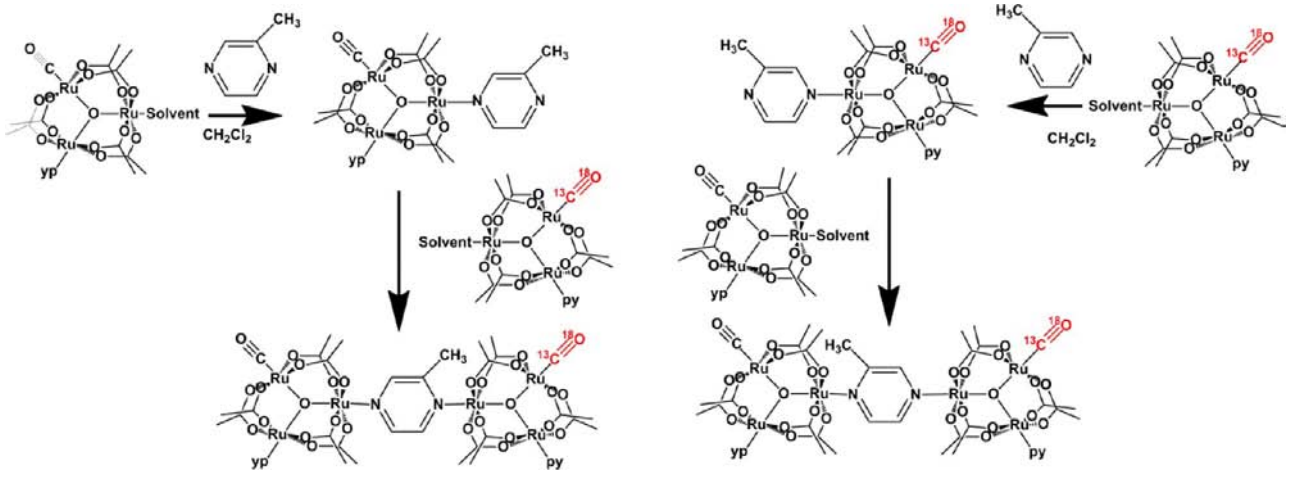

Figure 8. Synthetic scheme to prepare both regioisomers of the 2-mpz dimers of ruthenium trimers with $^{13}C^{18}O$ selectively located syn or anti to the 2-mpz methyl group.

$(OAc)_6(CO)(py)(\eta^1\text{-2-mpz})$, is then used as the "ligand" and combined with another 1 equiv of the solvento species, which now has a $^{13}C^{18}O$ ligand installed. This produces a regioisomer with the methyl group of the 2-mpz bridging ligand on the same side as the labeled $^{13}C^{18}O$. If the order of addition is reversed, another regioisomer with the 2-mpz methyl group pointing away from the label is obtained. The IRSEC responses in the usual 0/1−/2− redox states of both regioisomers prepared in this way are shown in Figure 9. First, consider the regioisomer with the 2-mpz methyl group syn to the labeled $^{13}C^{18}O$ (Figure 9, left). In the neutral state, the presence of $^{13}C^{18}O$ on one side of the complex and carbon monoxide on the other leads to the appearance of two bands in the ν(CO) spectrum shifted by ca. 90 cm^{-1} from the isotope mass differences. When the complex is doubly reduced to the 2− state, both of these isotope bands shift lower in energy by the usual ca. 40 cm^{-1} from the introduction of the charge, but they are still separated by ca. 90 cm^{-1}. The IRSEC response in the mixed-valence (1−) state shows *four* ν(CO) bands, two of major intensity and two of minor intesnsity. Those four bands correspond to the two ν(CO) spectra of the two different charge distributions possible in an asymmetric mixed-valence ion, weighted by their Boltzmann populations. The assignment of the spectra is straightforward. For the two bands of minor intensity, one is at the lowest frequency and the other at the highest frequency. This must correspond to the electronic charge residing on the Ru_3 cluster on the right side of the mixed-valence ion (Figure 9, left) because it both is nearest to the methyl group and contains $^{13}C^{18}O$. The lowest-frequency band must be perturbed in that direction by both isotope substitution and the presence of charge. The other side of this mixed-valence isomer is perturbed by neither charge nor isotope, and so it must be the origin of the highest-frequency band. The highest- and lowest-frequency bands have the same intensities because together they belong to the minor mixed-valence isomer. There is less of the minor isomer because it contains the electron on the stronger donor side of the 2-mpz ligand and is thus destabilized. The two more intense peaks of the four are then assigned to the major isomer. Note that, in moving from higher to lower energy, the pattern of intensities is minor−major−major−minor. Now consider the other regioisomer (Figure 9, right). Placing the 2-mpz methyl group on the opposite side of $^{13}C^{18}O$ reverses the preferred location of the electron with respect to the labeled $^{13}C^{18}O$ ligand in the minor and major isomers. Indeed, the pattern of four ν(CO) intensities is reversed to major−minor−minor−major in the anti regioisomer. The relative populations of the minor and major mixed-valence isomers described here are the same for both regioisomers (K = 2.2). The fact that the populations are so nearly equal is a clear indication that the perturbation to the

dx.doi.org/10.1021/ic302331s | *Inorg. Chem.* 2013, 52, 5663−5676

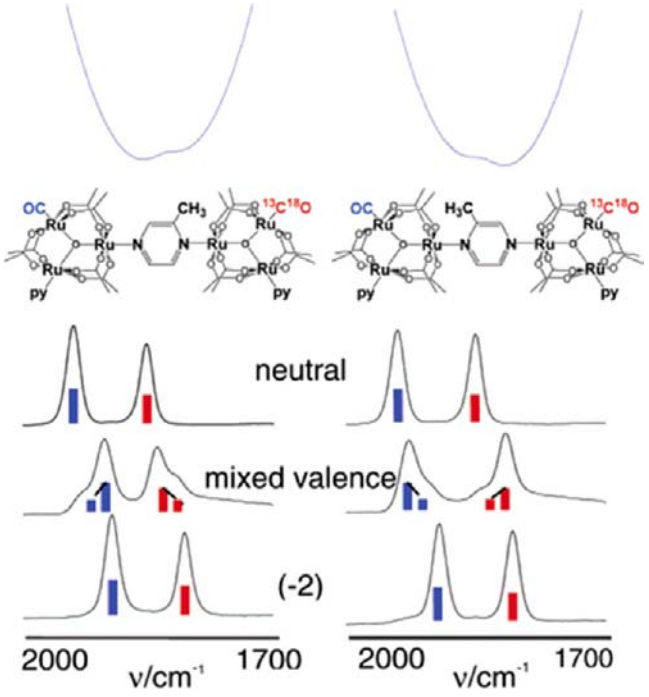

Figure 9. Qualitative potential energy surfaces showing the double minima of the major and minor isomer states and IRSEC spectra of the neutral (top), mixed-valence (middle), and doubly reduced (bottom) states shown with a schematic of the exchanging populations.

electronic structures caused by the asymmetric 2-mpz ligand is small and the electronic coupling H_{ab} huge.

Mixed-valence isomers have also been observed in complexes that are bridged by symmetric ligands but have asymmetric ancillary ligand substitution patterns.[60] This was achieved by preparing dimers with different pyridines (cpy, py, and dmap) on each side. In this case, the differences in mixed-valence isomer populations were found to be dependent on the differences in the pK_a values of the ancillary ligands on each side.[60] By integration of the ν(CO) intensities, the equilibrium constants for the partitioning of charge between the left and right sides can be determined. This allowed us to quantify the driving force for ET in an asymmetric mixed-valence ion in the strongly coupled adiabatic limit and to compare it to the driving force that arises only from asymmetric ligand substitution in the diabatic limit.[60] In general, cyclic voltammetry of a mixed-valence ion will show a splitting in the two reduction waves if electronic coupling is present. As the coupling is increased, this splitting will increase. If little or no coupling is present, no splitting will be apparent. It is important to recognize that each reduction wave represents the reduction of one of two interacting Ru_3 clusters and the intrinsic reduction potential of each cluster is the average (Figure 10).

In strongly coupled asymmetric mixed-valence ions, IR spectroscopy is used to determine the equilibrium constants for the relative populations of their mixed-valence isomers. The equilibrium constants in the diabatic (H_{ab} = 0) limit are then estimated from electrochemical data for corresponding symmetric complexes. Analysis of these data provides direct measurements of $\Delta\Delta G$, the difference in the thermodynamic stability of the two mixed-valence isomers in the diabatic and strongly coupled adiabatic limits (Figure 11). Here, ΔG_1 is defined as the free energy difference calculated from the mixed-

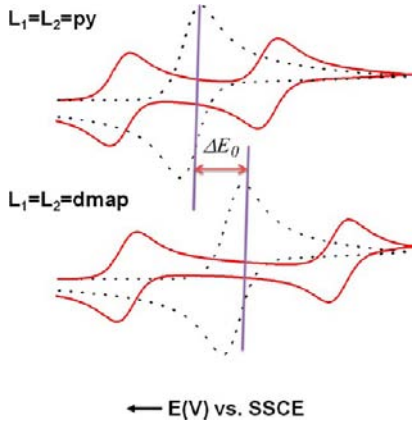

Figure 10. Comparison of the CVs for the 0/1− and 1−/2− couples of the pz-bridged dimers of ruthenium trimers having $L_1 = L_2$ = py and $L_1 = L_2$ = dmap, showing that for strongly coupled adiabatic mixed-valence ions the two waves (red) are symmetrically disposed around the reduction potential in the absence of coupling (black, dashed). The difference in the reduction potentials in the diabatic (H_{ab} = 0) limit for the py- and dmap-substituted dimers, ΔE_0, is then the difference in the average potentials for the 0/1− and 1−/2− couples.

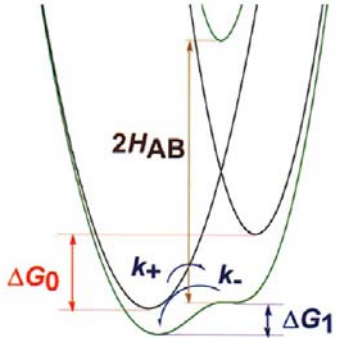

Figure 11. Potential energy surfaces for adiabatic and diabatic asymmetric systems. $\Delta\Delta G = \Delta G_0 - \Delta G_1$ is the *change* in the driving force caused by strong quantum mechanical mixing and delocalization in mixed-valence isomers.

valence isomer equilibrium constants measured by IR. This is the difference in energy between the two sides of a strongly coupled, asymmetric mixed-valence ion. Then, ΔG_0 is $-nF\Delta E_0$, where E_0 is the difference in the average reduction potentials of symmetric mixed-valence dimers with the respective ancillary pyridine ligands (Figure 10). This is the difference in the reduction potentials of differently substituted (dmap, py, cpy, etc.) Ru_3 clusters in pz-bridged dimer of trimer structures, if there were no electronic interactions (H_{ab} = 0). The values of $\Delta\Delta G = \Delta G_0 - \Delta G_1$ for three differently substituted asymmetric mixed-valence ions are summarized in Table 1. The most striking feature of this data is the enormous energy-leveling effect that arises from mixing of the diabatic states. This is a measure of the degree of delocalization. For example, differences in the electronic stability that are due to different pyridine ligand substitutions of as much as 1850 cm^{-1} (L_1 = cpy and L_2 = dmap) when there is no electron delocalization (ΔG_0) are reduced to 200 cm^{-1} (ΔG_1), *by delocalization*. The greatest degree of leveling is found to occur when the difference in the pyridine ligand donor ability is greatest (L_1 = cpy and L_2 = dmap) in the first place. $\Delta\Delta G$ values for the ligand sets with similar differences in the ligand donor ability (L_1 = py and L_2 =

dx.doi.org/10.1021/ic302331s | Inorg. Chem. 2013, 52, 5663−5676

Table 1. Comparison of the Free-Energy Differences between the Two Sides of Asymmetric Mixed-Valence Ions with Bridging pz and Differently Substituted Ancillary Ligands, L_1 and L_2, for the Strongly Coupled Adiabatic (ΔG_1) and Uncoupled Diabatic Cases (ΔG_0)[a]

L_1, L_2	K_{eq}	ΔG_1, cm^{-1}	ΔG_0, cm^{-1}	$\Delta\Delta G$, cm^{-1}
py, dmap	1.6	75	810	735
cpy, dmap	3.4	200	1850	1650
cpy, py	2.4	140	1050	910

[a] K_{eq} values were obtained by integration of IR bands of the mixed-valence isomers.

dmap; L_1 = cpy and L_2 = py) are less, but the adiabatic ΔG_1 values are still an order of magnitude less than the diabatic ΔG_0 values, showing how much deleocalization flattens and mixes the two sides of the potential energy surface. We have attempted to use the change in the thermodynamic stability of mixed-valence isomers in the strongly coupled adiabatic and uncoupled diabatic limits to estimate the electronic coupling.[63] The difference between ΔG_0 and ΔG_1 allows for the determination of H_{ab} from the thermodynamic parameters extracted from the electrochemistry of asymmetric mixed-valence ions. Because the potential energy surface and band minima are a function of H_{ab} and the total reorganizational energy in the symmetric case (λ_{symm}), H_{ab} can be described solely on the experimental quantities and expressed as eq 1.[63]

$$H_{ab} = \frac{\lambda_{symm}}{2\Delta G_0}\sqrt{(\Delta G_0)^2 - (\Delta G_1)^2} \quad (1)$$

Estimates of H_{ab} from eq 1 are much larger than those estimated by the method of Hush[2] (eq 2) and would place the mixed-valence ions described here as essentially completely delocalized (class III). Of course, the derivations of both eqs 1 and 2 are based on a two-state model of mixed valency, and we have seen the limitations of that model throughout this work.

$$H_{ab}{}^{*} = 2.06 \times 10^{-2}\frac{(\bar{\nu}_{max}\bar{\varepsilon}_{max}\bar{\nu}_{1/2})^{1/2}}{r} \quad (2)$$

ROLE OF SOLVENT DYNAMICS IN MIXED-VALENT GROUND STATES AND THE LOCALIZED-TO-DELOCALIZED TRANSITION

The very fast rate constants for intramolecular ET, estimated from IR line-shape analysis, and strongly delocalized ground states, observed in studies of mixed-valence isomers, suggest that the activation energy for ET in the Ru_3-pz-Ru_3 mixed-valence systems is near zero. The rate expression for ET in a symmetric mixed-valence complex with no driving force is given in eq 3.

$$k_{ET} = \kappa\nu_N \exp[-(\lambda/4 - H_{ab} + H_{ab}{}^2/\lambda)/RT] \quad (3)$$

One important disparity that has been noted previously concerns the rate constants calculated from eq 3 using values of H_{ab} calculated from the Hush equation (eq 2).[2,22] By making the typical assumptions, κ is 1 and ν_N is ca. 5.0×10^{12}, and using H_{ab} calculated from the IVCT band and eq 2, rate constants on the order of 10^9 s^{-1} were obtained.[22] This was troubling because the rate constants estimated from the coalescence of IR bands were on the order of 10^{12} s^{-1}. This disparity could be due to our inability to accurately measure the ET distance (r) in eq 2, but there are two reasons why this seems unlikely. First, the ET distance would have to be revised downward by nearly a factor of 4 to give H_{ab} values that give rate constants in agreement with experiment; second, the large shifts in ν(CO) of 40 cm^{-1} to lower energy that are observed for the reduced sides of the mixed-valence complexes are consistent with *metal-based* redox changes, and thus (long) values of r that reflect Ru−Ru separations seem more appropriate. Rate constants calculated using the thermodynamically derived values for H_{ab} of eq 1 are in much better agreement with experiment, on the order of 10^{12} s^{-1}, and are primarily governed by the nuclear frequency factor *preexponential terms*. This is easily seen because the values of H_{ab} from eq 1 approach values of $\lambda/2$, and in the limit $H_{ab} = \lambda/2$, eq 3 predicts an activation energy of *zero*.[63] It is unusual in most condensed-phase chemistry to work in a kinetic regime where rate constants are dominated by the preexponential terms, but this is completely consistent with two separate studies that we have undertaken of the effects of the solvent and medium on the rates of ET. In the first of these studies,[53] we showed that the rate constants estimated from the coalescing line shapes of the IR spectra (Figure 12) of symmetric mixed-valence complexes

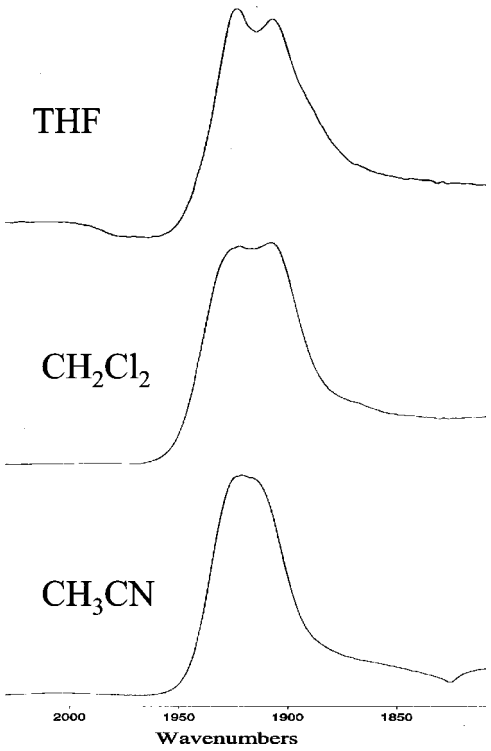

Figure 12. Solvent dependence of the IR line-shape coalescence in $\{[Ru_3O(OAc)_6(CO)(py)]_2\text{-pz}\}^-$ in different solvents. Intramolecular ET appears faster in the order CH_3CN > CH_2Cl_2 > THF.

1−**3** and BL = pz and L = 3-cpy are controlled by solvent dynamics. In particular, we demonstrated that the rate constants scale clearly with the dipolar solvent reorientation times determined by Maroncelli and co-workers, especially the fastest solvent response, t_{1e}.[64,65] The fastest solvent response is generally believed to involve mostly inertial rotation. Figure 13 compares the lifetimes ($k_{ET}{}^{-1}$) estimated from IR line-shape analysis of four mixed-valence ions in seven different solvents with the principal moments of inertia of the solvents. The correlation between the ET lifetimes and principal moments of inertia is strikingly good. This makes it clear that solvent

dx.doi.org/10.1021/ic302331s | Inorg. Chem. 2013, 52, 5663−5676

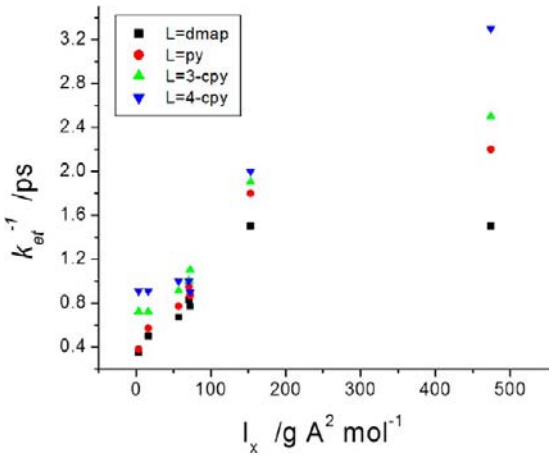

Figure 13. Comparison of the lifetimes (k_{ET}^{-1}) estimated from the IR line shapes of the four mixed-valence ions $\{[Ru_3O(OAc)_6(CO)(L)]_2\text{-}BL\}^{-1}$, where BL = pz and L = dmap (**1**), py (**2**), and 4-cpy (**3**) or 3-cpy versus the principal moments of inertia of seven solvents (MeCN, CH_2Cl_2, $CHCl_3$, THF, DMSO, DMF, and HMPA, left to right).

dynamics, not thermodynamics, is governing the rates of ET in these systems. It is important to note that solvent reorganization energies, λ_0, for the same seven solvents are strikingly uncorrelated with ET lifetimes.[19] Clearly, solvent dipolar reorientation times are important contributors to the nuclear frequency factor preexponential term, ν_N, in eq 3. The frequency factor, ν_N, is often described in ET reactions as the frequency at which inner- and outer-sphere modes are in configurations required by the conservation of energy for an electron to transfer from reactants to products.[19] Typically, the nuclear frequency factor is comprised of the weighted average of the nuclear frequencies for all of the modes that contribute to the ET reorganization energy (eq 4).

$$\nu_N = [\sum_i \nu_i^2 E_i / \sum_i E_i]^{1/2} \quad (4)$$

The relevant modes are the solvent frequencies and the intramolecular asymmetric ("promoter") vibrations that direct ET. Meyer et al. have discussed the effect that rigid media have on restricting solvent dipolar reorientation.[66] In a frozen medium, the solvent dipolar reorientation modes no longer play a dynamical role and ν_N *increases* from the ca. 10^{12} s^{-1} relaxation time of a typical organic solvent to ca. 10^{13} s^{-1}, the weighted average of intramolecular vibrations. This analysis leads to the curious prediction that, for rate expressions dominated by preexponential terms, the observed rate of intramolecular ET will *increase with decreasing temperature* but only at the point where the solvent medium becomes rigid. We have observed precisely this behavior with our systems. Our second study of the solvent dependence of our mixed-valence systems was based on the effects of temperature on the coalescence of ν(CO) bands, especially at the freezing point of the solvents.[18,19] The temperature dependences of the ν(CO) spectrum of $\{[Ru_3O(OAc)_6(CO)(cpy)]_2\text{-}pz\}^-$ in CH_2Cl_2 and MeCN solutions are compared in Figure 14. In both solvents, the ν(CO) spectra show minor coalescence, until near the respective solvent freezing points, a marked increase in the coalescence is observed. Below the respective freezing points, the band shapes do not change further. The rate constants obtained from the ν(CO) spectral line shapes below the freezing points of the two different solvents are the same, even though they are quite different at room temperature (Figure 14). These results demonstrate a localized-to-delocalized transition at the freezing point of the solvents, where solvent dynamics become largely uncoupled from ET and internal vibrational modes of the molecule take over as the dominant frequencies involved in ET. What cannot be determined from these IR experiments is whether this localized-to-delocalized transition represents only the transition from ET dynamics that are restricted by solvent motion to ET dynamics that are restricted by internal modes of vibration or whether it is the transition to the ultimate state of delocalization. These questions were better addressed by studies of the temperature and solvent dependence of the IVCT bands in the three-state mixed-valence model. From spectroscopic studies in different solvents and at different temperatures, we were able to refine further our understanding of the behavior of mixed-valence complexes at the class II/III borderline.[17] IVCT spectra of $\mathbf{1}^-$–$\mathbf{3}^-$ were weakly solvent-dependent, indicating that these mixed-valence systems are deeply adiabatic. Changes in the IVCT bands of $\mathbf{1}^-$–$\mathbf{4}^-$ in acetonitrile and methylene chloride were followed as a function of the temperature. Figure 15 shows the

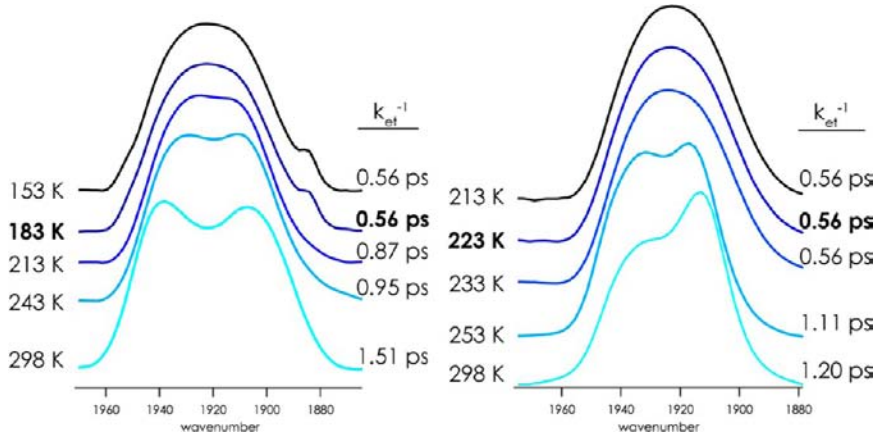

Figure 14. IR band shape for ν(CO) of the mixed-valence dimer $\{[Ru_3O(OAc)_6(CO)(cpy)]_2\text{-}pz\}^-$ in methylene chloride (left) and acetonitrile (right) as a function of the temperature. Increasing coalescence in the band shape is observed as the freezing point of the solution (183 and 223 K, respectively) is approached. To the right of each spectrum are listed the ET lifetimes obtained from simulation of the corresponding spectrum. Interestingly, both solvents yield the same ET lifetime (0.56 ps) as the solvent is frozen.

dx.doi.org/10.1021/ic302331s | *Inorg. Chem.* 2013, 52, 5663–5676

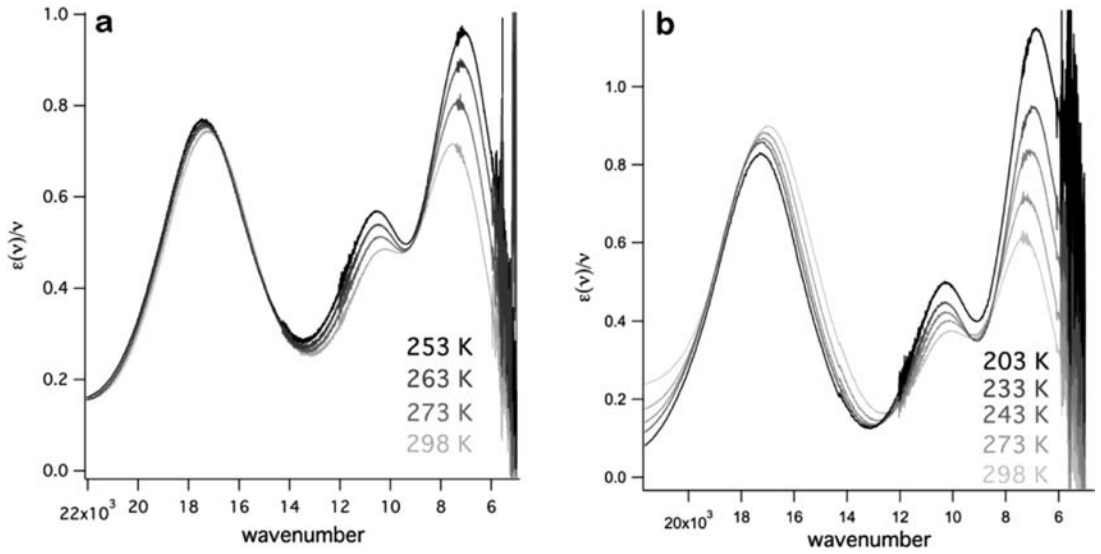

Figure 15. Spectra of 3^- collected in acetonitrile (a) and methylene chloride (b). An increase in MBCT and decrease in MMCT band energies are observed in both solvents.

spectra of 3^- in acetonitrile and methylene chloride at increasingly colder temperatures. As the temperature is decreased, the bands intensify and change in energy. Specifically, the MMCT transition decreases in energy and the MBCT transition increases in energy. The divergence in energies of the two transitions is reminiscent of the behavior exhibited by 1^-–4^- as electronic communication increases (vide supra) with the ancillary ligand donor ability. This trend is consistent with increasingly delocalized behavior as the temperature is decreased. Additionally, the MMCT bands increase in intensity by nearly 50% in acetonitrile and by over a factor of 2 in methylene chloride (Figure 15). An increase in the intensity of the MMCT band is predicted by the three-state model for a system that is approaching delocalization.[13,17] This observation of increasingly delocalized behavior as the temperature decreases is in accord with our observations of the temperature dependence on ground-state ET in IR studies of the ν(CO) spectra, described above. In comparison, the IVCT spectra of the most strongly coupled system 1^- in acetonitrile at increasingly colder temperatures show intensification of the MMCT band and *weakening* of the MBCT band, consistent with a class II/III to class III transition.[17] This system also undergoes dramatic changes in intensity, a 90% increase in MMCT and a 20% *decrease* in MBCT.

Changing the reorganization energy in a mixed-valence system will alter the landscape of its potential energy surfaces. Increasing the reorganization energy and treating H_{ad}, H_{ac}, and ΔG_{ac} as constants will cause the activation barrier along the symmetric coordinate to increase, and a mixed-valence species will take on more localized character. Conversely, decreasing the reorganization energy will allow a mixed-valence species to take on more delocalized character. All other factors being equal, when the reorganization energy is smaller, the potential energy surface is more adiabatic. The IVCT spectra of 1^-–3^- are consistent with small decreases in the reorganization energy as the temperature is decreased[17] (Figure 15).

For systems that are described well by a three-state semiclassical model such as the mixed-valence complexes 1^-–4^- considered here, it became clear that delocalization on the time scale of the fastest (inertial) solvent motions is not sufficient to achieve complete electronic delocalization. Complexes 1^-–4^- exhibit such a well-behaved and predictable (by the three-state model) progression through the class II/III borderline that it is tempting to use criteria from the three-state model to assign a particular system's behavior to either an "early" or "late" class II/III borderline. One trend that becomes immediately clear is that, within the three-state description energies of MMCT and MBCT, bands diverge with increased electronic communication. This relationship can be used to compare a series of mixed-valence complexes with varying degrees of electronic coupling, especially if the value of the electronic coupling constant is not explicitly known, as is often the case in highly electronically coupled complexes. We have also found from studies of the solvent and temperature dependences that different types of behavior can be observed in the class II/III borderline region. For example, the bipy-bridged complex 4^- displays temperature independence in its IVCT electronic spectra as well as in its ν(CO) spectrum. It is clearly a class II mixed-valence system, but it sits near the entry to class II/III borderline systems. As a mixed-valence system enters the "early" class II/III borderline regime, the influence of dynamic contributions from the solvent becomes evident. Vibrational *and* optical investigations of 2^- and 3^- reveal solvent and temperature dependences. The ν(CO) spectra show two resolved bands at room temperature, and these bands coalesce at the solvent freezing points to apparently more delocalized states, no longer dependent on the solvent motions that are slower than the maximum rate of ET (Figure 14). This view is reinforced by the temperature dependence of the IVCT spectra of 2^- and 3^-, which show MBCT bands moving to higher energy and MMCT bands moving to lower energy and gaining significant intensity as the temperature is lowered (Figure 15). As mixed-valence system transition through the later phases of class II/III borderline behavior to class III, solvent and temperature dependences of ET wane, as in 1^-. Thus, complexes 1^-–4^- represent discrete points on a nearly complete class II to class III transition. In the class II complex 4^-, solvent dynamics are too fast to affect ET. In the (nearly) class III complex 1^-, solvent dynamics are too slow to affect ET. The class II/III borderline complexes 2^- and 3^- show the

dx.doi.org/10.1021/ic302331s | *Inorg. Chem.* 2013, 52, 5663–5676

strongest correlation with solvent dynamics, particularly Manoncelli's t_{1e}. Two key points learned from the investigation of these mixed-valence systems are as follows: (1) solvent dynamics tend to localize otherwise delocalized states, and (2) delocalization on the time scale of the fastest (inertial) solvent motions is not sufficient to achieve complete electronic delocalization. This is a result of solvent dynamics becoming nearly irrelevant as the rate of ET becomes significantly faster than the solvent response. This study has thus provided guidelines for establishing where a particular system lies within the border region and criteria that can be applied more widely to "late" class II, class II/III borderline, "late" borderline, and class III. Jortner, Hynes, and others have provided detailed theoretical models for including solvent dynamics in Marcus-type descriptions of ET.[67−71] A recent study by Matyushov was the first to report strong correlations between solvent-dynamical theoretical models of nonergodic ET and our experimental work.[72]

CONCLUDING REMARKS

The field of inorganic mixed valency has greatly evolved since the 1960s, and many questions remain that are not fully understood. Work in our laboratory has focused on using the coalescence of ν(CO) band shapes in the 1D IR spectra of mixed-valence complexes of the type $\{[Ru_3O(OAc)_6(CO)(L)]_2\text{-BL}\}^-$, where L = a pyridyl ligand and BL = pz or bipy, to determine the rate constants of ET in solution and to further understand such a simple chemical reaction. During this time, these systems have allowed us to understand the medium and environmental effects on ET dynamics by spectroscopic studies. Studies of these mixed-valence complexes have provided a clear picture of ET dynamics at the class II/III borderline delocalization, as well as a more precise definition of the borderline behavior. Utilizing these dynamic systems, we proposed a revised definition of class II/III borderline mixed-valence complexes: the solvent-dynamical parameters control the rates of ET and tend to localize otherwise delocalized states.[19]

We have learned much in 16 years of study of mixed valency in the dimer of trimer Ru_3 systems. This article has faithfully followed the presentation of topics in the ACS Award in Inorganic Chemistry Award Address, March 2012. What the author had hoped to do at that time was to cover a few of the future directions of research in this field, but time did not allow him to do so. Therefore, some of the most recent work and future directions are mentioned briefly here. The future of this field is headed in the direction of mixed valency in supramolecular systems and molecular electronics. The fundamental idea of a mixed-valence complex existing as an electronically bistable system that could, in principle, be switched on the picosecond time scale is a compelling molecular device concept.[73] Mixed valency across hydrogen bonds was described recently,[74] and this is being investigated further to study the dynamics of proton-coupled ET reactions. Electron delocalization across a supramolecular assembly also appears to be a promising method to harden soft, noncovalent interactions.[75] Mixed-valence nanoclusters[76−78]—supramolecular assemblies of redox-active metal centers exchanging electrons through metallic or semiconducting nanoclusters—are also promising systems for achieving efficient photochemical charge separation.

AUTHOR INFORMATION

Corresponding Author

*E-mail: ckubiak@ucsd.edu.

Notes

The authors declare no competing financial interest.

Biography

Clifford P. Kubiak received a Sc.B. degree with honors in chemistry from Brown University (1975) and a Ph.D. (1980) in chemistry from the University of Rochester, where he worked with Richard Eisenberg. He was a postdoctoral associate with Mark S. Wrighton at Massachusetts Institute of Technology (1980−1981). He was a faculty member at Purdue University from 1982 to 1998. He moved to University of California—San Diego (UCSD) in 1998 as a Harold C. Urey Professor. He was named Distinguished Professor at UCSD in 2008. He has held visiting appointments at Tohoku University, University of Chicago, and University of Erlangen. He was the recipient of the ACS Award in Inorganic Chemistry (2012) and was selected as a Fellow of the ACS (2012). He has served on the Editorial Advisory Boards of *Accounts of Chemical Research*, *Inorganic Chemistry*, and *Materials Science in Semiconductor Processing*. He is the author of over 200 scientific articles. His research is in CO_2 fixation and utilization and ultrafast electron transfer within the ground states of inorganic mixed-valence systems, which is the topic described in this article.

ACKNOWLEDGMENTS

C.P.K. acknowledges a most rewarding collaboration with Prof. Tasuko Ito (now retired) and his co-workers at Tohoku University and thanks the many students and co-workers, first at Purdue University, and then at UCSD who continued to find new layers of interesting detail in the electronic structures,

spectroscopy, dynamics, and syntheses of Ru_3 cluster mixed-valence systems. He also thanks current students Gabe Canzi and Jane Henderson for valuable assistance in preparing the manuscript and acknowledges the NSF for funding of the research presented here. This article is dedicated to Dr. Norman Sutin of Brookhaven National Laboratory for his landmark contributions to the field of inorganic mixed valency and, through his publications over many years, for his profound influence on the thinking of the author in the work described here.

REFERENCES

(1) Creutz, C.; Taube, H. *J. Am. Chem. Soc.* **1969**, *91*, 3988−3989.
(2) Hush, N. S. *Prog. Inorg. Chem.* **1967**, *8*, 391.
(3) Marcus, R. A.; Sutin, N. *Biochim. Biophys. Acta* **1985**, *8111*, 265−322.
(4) Sutin, N. *Prog. Inorg. Chem.* **1983**, *30*, 441−498.
(5) Robin, M. B.; Day, P. *Adv. Inorg. Chem. Radiochem.* **1967**, *10*, 247.
(6) Brunschwig, B. S.; Sutin, N. *Coord. Chem. Rev.* **1999**, *187*, 233−254.
(7) Chisholm, M. H. *Proc. Natl. Acad. Sci. U.S.A.* **2007**, *104*, 2563−2570.
(8) D'Alessandro, D. M.; Keene, F. R. *Chem. Soc. Rev.* **2006**, *35*, 424−440.
(9) Demadis, K. D.; Hartshorn, C. M.; Meyer, T. J. *Chem. Rev.* **2001**, *101*, 2655−2685.
(10) Oh, D. H.; Sano, M.; Boxer, S. G. *J. Am. Chem. Soc.* **1991**, *113*, 6880−6890.
(11) Ondrechen, M. J.; Ko, J.; Zhang, L. T. *J. Am. Chem. Soc.* **1987**, *109*, 1672−1676.
(12) Reimers, J. R.; Hush, N. S. *Chem. Phys.* **1996**, *208*, 177−193.
(13) Brunschwig, B. S.; Creutz, C.; Sutin, N. *Chem. Soc. Rev.* **2002**, *31*, 168−184.
(14) D'Alessandro, D. M.; Topley, A. C.; Davies, M. S.; Keene, F. R. *Chem.—Eur. J.* **2006**, *12*, 4873−4884.
(15) Glover, S. D.; Goeltz, J. C.; Lear, B. J.; Kubiak, C. P. *Eur. J. Inorg. Chem.* **2009**, 585−594.
(16) Glover, S. D.; Goeltz, J. C.; Lear, B. J.; Kubiak, C. P. *Coord. Chem. Rev.* **2010**, *254*, 331−345.
(17) Glover, S. D.; Kubiak, C. P. *J. Am. Chem. Soc.* **2011**, *133*, 8721−8731.
(18) Glover, S. D.; Lear, B. J.; Salsman, C.; Londergan, C. H.; Kubiak, C. P. *Philos. Trans. R. Soc. A* **2008**, *366*, 177−185.
(19) Lear, B. J.; Glover, S. D.; Salsman, J. C.; Londergan, C. H.; Kubiak, C. P. *J. Am. Chem. Soc.* **2007**, *129*, 12772−12779.
(20) Chisholm, M. H.; Patmore, N. J. *Acc. Chem. Res.* **2006**, *40*, 19−27.
(21) Ito, T.; Hamaguchi, T.; Nagino, H.; Yamaguchi, T.; Washington, J.; Kubiak, C. P. *Science* **1997**, *277*, 660−603.
(22) Ito, T.; Hamaguchi, T.; Nagino, H.; Yamaguchi, T.; Kido, H.; Zavarine, I. S.; Richmond, T.; Washington, J.; Kubiak, C. P. *J. Am. Chem. Soc.* **1999**, *121*, 4625−4632.
(23) Haines, R. J.; Wittrig, R. E.; Kubiak, C. P. *Inorg. Chem.* **1994**, *33*, 4723−4728.
(24) Morgenstern, D. A.; Ferrence, G. M.; Washington, J.; Henderson, J. I.; Rosenhein, L.; Heise, J. D.; Fanwick, P. E.; Kubiak, C. P.; Kubiak, P. *J. Am. Chem. Soc.* **1996**, *118*, 2198−2207.
(25) Washington, J.; Kubiak, C. P. *Can. J. Chem.* **1996**, *74*, 2503−2508.
(26) Wittrig, R. E.; Kubiak, C. P. *J. Electroanal. Chem.* **1995**, *393*, 75−86.
(27) Abe, M.; Sasaki, Y.; Yamada, Y.; Tsukahara, K.; Yano, S.; Ito, T. *Inorg. Chem.* **1995**, *34*, 4490−4498.
(28) Abe, M.; Sasaki, Y.; Yamada, Y.; Tsukahara, K.; Yano, S.; Yamaguchi, T.; Tominaga, M.; Taniguchi, I.; Ito, T. *Inorg. Chem.* **1996**, *35*, 6724−6734.
(29) *Dynamic NMR Spectrosopy*; Jackman, L. M., Cotton, F. A., Eds.; Academic Press: New York, 1975; p 45.
(30) MacPhail, R. A.; Strauss, H. L. *J. Chem. Phys.* **1985**, *82*, 1156.
(31) Grevels, F.-W.; Jacke, J.; Klotzbücher, W. E.; Krüger, C.; Seevogel, K.; Tsay, Y. H. *Angew. Chem., Int. Ed. Engl.* **1987**, *26*, 885.
(32) Grevels, F.-W.; Kerpen, K.; Klotzbücher, W. E.; McClung, R. E. D.; Russell, G.; Viotte, M.; Schaffner, K. *J. Am. Chem. Soc.* **1998**, *120*, 10423−10433.
(33) Turner, J. J.; Gordon, C. M.; Howdle, S. M. *J. Phys. Chem.* **1995**, *99*, 17532−17538.
(34) Turner, J. J.; Grevels, F. W.; Howdle, S. M.; Jacke, J.; Haward, M. T.; Klotzbucher, W. E. *J. Am. Chem. Soc.* **1991**, *113*, 8347−8353.
(35) Montri, L.; Cannon, R. D. *Spectrochim. Acta A* **1985**, *41*, 643−646.
(36) White, R. P.; Wilson, L. M.; Williamson, D. J.; Moore, G. R.; Jayasooriya, U. A.; Cannon, R. D. *Spectrochim. Acta A* **1990**, *46*, 917−920.
(37) Wu, R.; Jayasooriya, U. A.; Cannon, R. D. *Spectrochim. Acta A* **2000**, *56*, 575−579.
(38) Wilking, J. N.; Manning, C. J.; Arbuckle-Keil, G. A. *Appl. Spectrosc.* **2004**, *58*, 304−312.
(39) Zheng, J.; Kwak, K.; Asbury, J.; Chen, X.; Piletic, I.; Fayer, M. D. *Science* **2005**, *309*, 1338−1343.
(40) Zheng, J.; Kwak, K.; Fayer, M. D. *Acc. Chem. Res.* **2006**, *40*, 75−83.
(41) Cervetto, V.; Helbing, J.; Bredenbeck, J.; Hamm, P. *J. Chem. Phys.* **2004**, *121*, 5935−5942.
(42) Hamm, P.; Lim, M.; DeGrado, W. F.; Hochstrasser, R. M. *Proc. Natl. Acad. Sci.* **1999**, *96*, 2036−2041.
(43) Barbour, L. W.; Hegadorn, M.; Asbury, J. B. *J. Am. Chem. Soc.* **2007**, *129*, 15884−15894.
(44) Cahoon, J. F.; Kling, M. F.; Sawyer, K. R.; Andersen, L. K.; Harris, C. B. *J. Mol. Struct.* **2008**, *890*, 328−338.
(45) Rubtsov, I. V.; Kang, Y. K.; Redmore, N. P.; Allen, R. M.; Zheng, J.; Beratan, D. N.; Therien, M. J. *J. Am. Chem. Soc.* **2004**, *126*, 5022−5023.
(46) Rubtsov, I. V.; Redmore, N. P.; Hochstrasser, R. M.; Therien, M. J. *J. Am. Chem. Soc.* **2004**, *126*, 2684−2685.
(47) Xiong, W.; Laaser, J. E.; Paoprasert, P.; Franking, R. A.; Hamers, R. J.; Gopalan, P.; Zanni, M. T. *J. Am. Chem. Soc.* **2009**, *131*, 18040−18041.
(48) de la Rosa, R.; Chang, P. J.; Salaymeh, F.; Curtis, J. C. *Inorg. Chem.* **1985**, *24*, 4229−4231.
(49) Dong, Y. H.; Hupp, J. T. *Inorg. Chem.* **1992**, *31*, 3170−3172.
(50) Richardson, D. E.; Taube, H. *Coord. Chem. Rev.* **1984**, *60*, 107.
(51) Sutton, J. E.; Taube, H. *Inorg. Chem.* **1981**, *20*, 3126−3134.
(52) Salsman, J. C.; Ronco, S.; Londergan, C. H.; Kubiak, C. P. *Inorg. Chem.* **2006**, *45*, 547−554.
(53) Londergan, C. H.; Salsman, J. C.; Ronco, S.; Dolkas, L. M.; Kubiak, C. P. *J. Am. Chem. Soc.* **2002**, *124*, 6236−6237.
(54) McClung, R. E. D. *VIBEX GL: A program for the simulation of IR spectra of exchanging systems.*
(55) Londergan, C. H.; Salsman, J. C.; Ronco, S.; Kubiak, C. P. *Inorg. Chem.* **2003**, *42*, 926−928.
(56) Londergan, C. H.; Rocha, R. C.; Brown, M. G.; Shreve, A. P.; Kubiak, C. P. *J. Am. Chem. Soc.* **2003**, *125*, 13912−13913.
(57) Rocha, R. C.; Brown, M. G.; Londergan, C. H.; Salsman, J. C.; Kubiak, C. P.; Shreve, A. P. *J. Phys. Chem. A* **2005**, *109*, 9006−9012.
(58) Rocha, R. C.; Shreve, A. P. *Chem. Phys.* **2006**, *326*, 24−32.
(59) Londergan, C. H.; Kubiak, C. P. *J. Phys. Chem. A* **2003**, *107*, 9301−9311.
(60) Ito, T.; Imai, N.; Yamaguchi, T.; Hamaguchi, T.; Londergan, C. H.; Kubiak, C. P. *Angew. Chem., Int. Ed.* **2004**, *43*, 1376−1381.
(61) Salsman, J. C.; Kubiak, C. P.; Ito, T. *J. Am. Chem. Soc.* **2005**, *127*, 2382−2383.
(62) Goeltz, J. C.; Glover, S. D.; Hauk, J.; Kubiak, C. P. In *Inorganic Synthesis*; Rauchfuss, T. B., Ed.; Wiley: New York, 2010; Vol. *35*; p 156.
(63) Londergan, C. H.; Salsman, J. C.; Lear, B. J.; Kubiak, C. P. *Chem. Phys.* **2006**, *324*, 57−62.

(64) Horng, M. L.; Dahl, K. G. J., II; Maroncelli, M. *Chem. Phys. Lett.* **1999**, *315*, 363−370.
(65) Horng, M. L.; Gardecki, J. A.; Papazyan, A.; Maroncelli, M. *J. Phys. Chem.* **1995**, *99*, 17311−17337.
(66) Chen, P.; Meyer, T. J. *Inorg. Chem.* **1996**, *35*, 5520−5524.
(67) Bixon, M.; Jortner, J. *Chem. Phys.* **1993**, *176*, 467−481.
(68) Kim, H. J.; Hynes, J. T. *J. Phys. Chem.* **1990**, *94*, 2736−2740.
(69) Rips, I.; Klafter, J.; Jortner, J. *J. Phys. Chem.* **1990**, *94*, 8557−8561.
(70) Smith, B. B.; Staib, A.; Hynes, J. T. *Chem. Phys.* **1993**, *176*, 521−537.
(71) Zichi, D. A.; Ciccotti, G.; Hynes, J. T.; Ferrario, M. *J. Phys. Chem.* **1989**, *93*, 6261−6265.
(72) Matyushov, D. V. *J. Phys. Chem. Lett.* **2012**, *3*, 1644−1648.
(73) Lear, B. J.; Kubiak, C. P. *Inorg. Chem.* **2006**, *45*, 7041−7043.
(74) Goeltz, J. C.; Kubiak, C. P. *J. Am. Chem. Soc.* **2010**, *132*, 17390−17392.
(75) Lear, B. J.; Kubiak, C. P. *J. Phys. Chem. B* **2007**, *111*, 6766−6771.
(76) Canzi, G.; Kubiak, C. P. *Small* **2011**, *7*, 1967−1971.
(77) Canzi, G.; Kubiak, C. P. *J. Phys. Chem. C* **2012**, *116*, 6560−6566.
(78) Morris-Cohen, A. J.; Aruda, K. O.; Rasmussen, A. M.; Canzi, G.; Seideman, T.; Kubiak, C. P.; Weiss, E. A. *Phys. Chem. Chem. Phys.* **2012**, *14*, 13794−13801.